Supplementary Information for

Sub-milliwatt, widely-tunable coherent microcomb generation with feedback-free operation

Haowen Shu[1,6], Lin Chang[2,6], Chenghao Lao[3,6], Bitao Shen[1,6], Weiqiang Xie[2], Xuguang Zhang[1], Ming Jin[1], Yuansheng Tao[1], Ruixuan Chen[1] Zihan Tao[1], Huajin Chang[1], Shaohua Yu[1,4], Qi-Fan Yang[3,5], Xingjun Wang[1,4,5,†] and John E. Bowers[2,‡]

[1]State Key Laboratory of Advanced Optical Communications System and Networks, School of Electronics, Peking University, Beijing, 100871, China.

[2]Department of Electrical and Computer Engineering, University of California, Santa Barbara, CA 93106, USA.

[3]State Key Laboratory for Artificial Microstructure and Mesoscopic Physics, School of Physics, Peking University, Beijing 100871, China.

[4]Peng Cheng Laboratory, Shenzhen 518055, China.

[5]Frontiers Science Center for Nano-optoelectronics, Peking University, Beijing 100871, China.

[6]These authors contributed equally to this work.

Corresponding authors: [†]xjwang@pku.edu.cn, [‡]bowers@ece.ucsb.edu.

Supplementary note I: Statistical study of the high-Q resonators

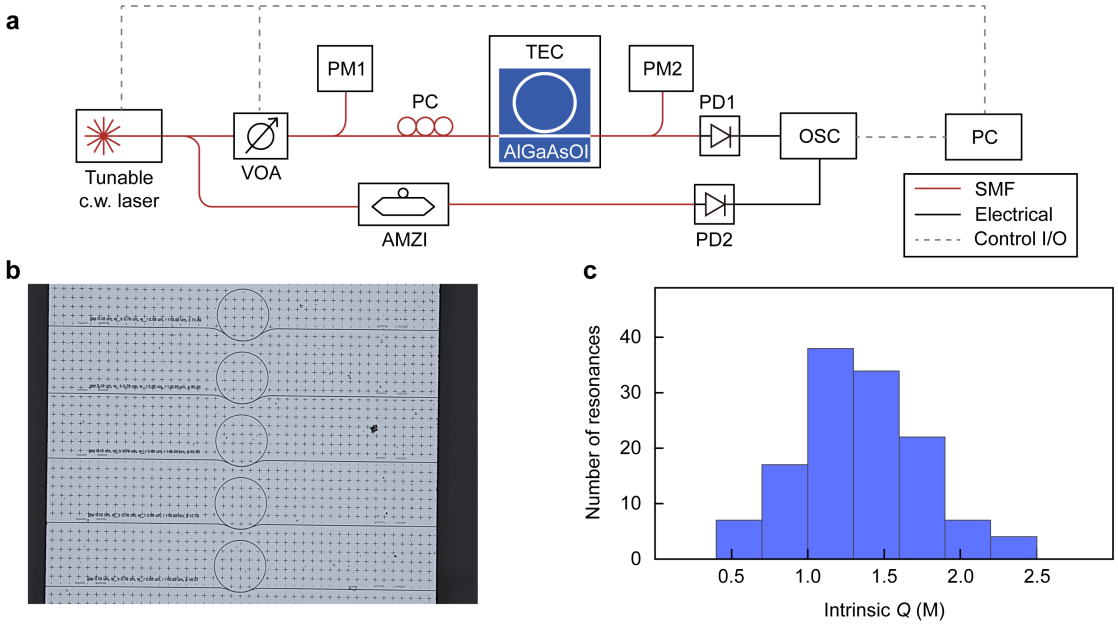

Supplementary Fig. S1: Q-factors measurement. **a**, Experimental setup. **b**, 5 of measured ring resonators in same waveguide dimensions with different coupling strength. **c**, Intrinsic Q-factors distribution of microresonators shown in figure b. The resonances at C band (1530∼1565 nm) are picked for the statistical analysis.

Supplementary Fig. S1a shows the measurement setup, which consists of two channels measured simultaneously in an oscilloscope. An external cavity diode laser is employed for wavelength scanning with no mode hoping. The power of the tunable laser is equally split into two channels. An variable optical attenuator (VOA) is deployed before laser injected into AlGaAs resonator. The transmission spectra are recorded when laser frequency is swept from 1530 to 1565 nm (C-band). Meanwhile, a fibre-based asymmetric MZI are constructed at the other channel for wavelength calibration. In our work, Q-factors in rings with identical waveguide dimensions in the same chip bar are charaterized, as shown in Supplementary Fig. S1b. Thanks to the optimized fabrication process, high-Q resonance can be reproducibly achieved in this III-V platform. The statistical analysis of intrinsic Q factors at C-band with identical ring dimensions is Supplementary Fig. S1c from which clusters range from 1 to 2 million can be observed.

Supplementary note II: Dark pulse supported by sub-milliwatt pump power

In order to give a better insight into the avoided-mode-crossing influenced self-stimulation of the dark-pulse in our devices, two mode families are considered here. One mode family is the dark-pulse-supporting mode family, referred as primary (P) mode family, and the other mode family is referred as auxiliary (A) mode family. The avoided-mode-crossing between the two mode families strongly modified the local dispersion, facilitating the self-stimulation of dark-pulses. The linear coupling between the primary modes and auxiliary modes is introduced into the LLEs:

$$\begin{aligned} t_R\frac{\partial E^{(P)}(t,\tau)}{\partial t} = &\left[-\left(\alpha^{(P)}-it_R\delta\right)+iL\frac{\beta_2^{(P)}}{2}\frac{\partial^2}{\partial\tau^2}\right]E^{(P)} \\ &+iL\gamma^{(P)}\left|E^{(P)}\right|^2E^{(P)}+iL\kappa E^{(A)}+\sqrt{\theta}E_{in} \end{aligned} \tag{S1}$$

$$\begin{aligned} t_R\frac{\partial E^{(A)}(t,\tau)}{\partial t} = &\left[-\left(\alpha^{(A)}-it_R\delta-i\Delta\right)+iL\frac{\beta_2^{(A)}}{2}\frac{\partial^2}{\partial\tau^2}\right]E^{(A)} \\ &+iL\gamma^{(A)}\left|E^{(A)}\right|^2E^{(A)}+iL\kappa E^{(P)} \end{aligned} \tag{S2}$$

$E^{(P)}$ and $E^{(A)}$ respectively stand for the intracavity temporal fields in the primary and the auxiliary modes, $\alpha^{(P)}=0.0067$ and $\alpha^{(A)}=0.02$ are the roundtrip cavity loss factor, $\beta_2^{(P)}$=139 ps^2 km^{-1} and $\beta_2^{(A)}$=-2421 ps^2 km^{-1} represent the second-order dispersion coefficients, and $\delta=\omega_0^{(P)}-\omega_p$ is the detuning, where $\omega_0^{(P)}$ is the resonance frequency of the primary mode and ω_p is the frequency of the pump field. t_R=11.628 ps is the roundtrip time of the primary mode and L=2$\pi\times$144 μm is roundtrip length. The pump filed is coupled into the primary mode by $\sqrt{\theta}E_{\text{in}}$, where θ=0.0067 is the waveguide coupling coefficient and E_{in} is the pump field. While the coupling between the pump field and the auxiliary mode is ignored, due to the relatively small coupling rate in the pulley couplers. $\gamma^{(P)}$=340 m^{-1} W^{-1} and $\gamma^{(A)}$=330 m^{-1} W^{-1} are the nonlinear coefficients. The linear coupling between two mode families is induced by $iL\kappa E^{(x)}(x=A,P)$, where κ=84 m^{-1} is linear coupling strength. Δ indicates the resonant frequency difference between the two modes, which is equal to $t_R\left[\left(\omega_0^{(A)}-\omega_0^{(P)}\right)-i\left(\beta_1^{(A)}-\beta_1^{(P)}\right)\frac{\partial}{\partial\tau}\right]$, where $\omega_0^{(A)}$ is the resonance frequency, $\beta_1^{(P)}$=12.280 ns/m and $\beta_1^{(A)}$=13.438 ns/m are the first-order dispersion coefficients. All paramaters used for simulation can be extracted from the experiment data. The $\omega_0^{(A)}-\omega_0^{(P)}$ is tuned to simulate the change of AMX. To get the results shown in Fig. 2b of the main text, the $t_R\left(\omega_0^{(A)}-\omega_0^{(P)}\right)$ is set to 0.81. In Fig. 2d of the main text, the $t_R\left(\omega_0^{(A)}-\omega_0^{(P)}\right)$ is set to

-0.01, -1.40, -1.96 and -2.49 for dark-pulses with different FSR.

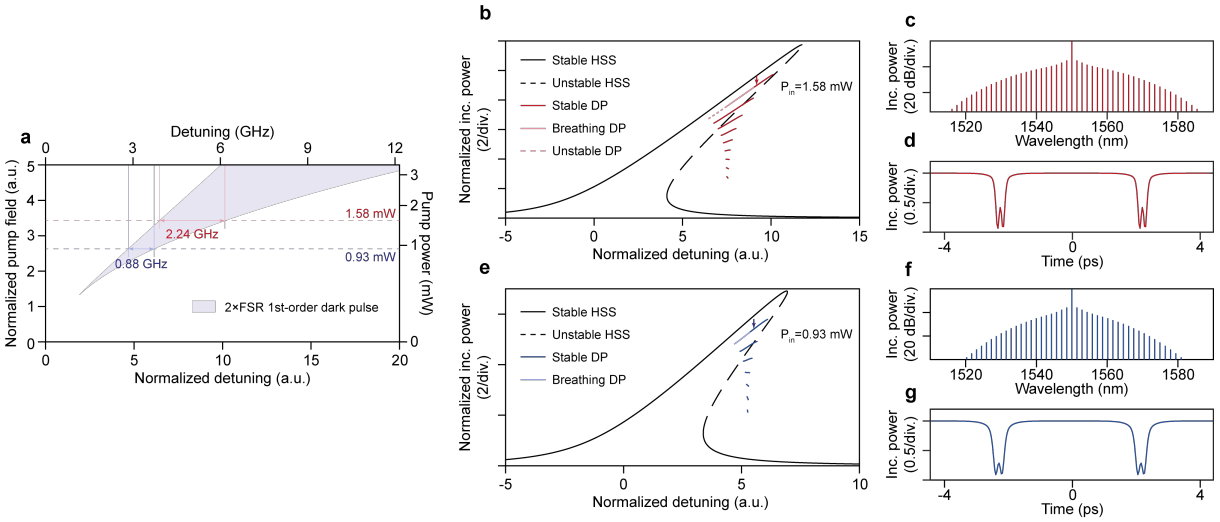

Supplementary Fig. S2: Existence regions and waveforms of 2×FSR dark pulses. **a**, the region of existence of 2×FSR 1st-order dark pulse in the (θ, ρ) parameter space, where θ and ρ represent the normalized detuning and the normalized pump power respectively. The red line and blue line represent pump powers of 1.58 mW and 0.93 mW. **b,e**, the steps of existence of different 2×FSR dark pulses for the pump power P_{in}=1.58 mW and 0.93 mW. **c,f**, simulated spectra of 2×FSR 1st-order dark pulse with P_{in}=1.58 mW and 0.93 mW and the dutuning marked by arrows shown in d and e. **d,g**,simulated waveforms in time domain with P_{in}=1.58 mW and 0.93 mW.

Different from the above numerical simulation for AMX analyze, a single LLE is employed to illustrate the situation of generating dark pulses with sub-milliwatt in AlGaAsOI microresonaters. Based on the mean field approximate, the evolution of the intracavity electric field can be described by

$$t_R\frac{\partial E(t,\tau)}{\partial t}=\left[-(\alpha-it_R\delta)+iL\frac{\beta_2}{2}\frac{\partial^2}{\partial\tau^2}\right]E+iL\gamma|E|^2E+iL\kappa E+\sqrt{\theta}E_{in} \tag{S3}$$

Where the symbol definition is same with that in Methods. By normalizing the Eq. S3, we can get a dimensionless mean-field LLE:

$$\frac{\partial}{\partial t'}A=-(1+i\theta)A-i\frac{\partial^2}{\partial x^2}A+i|A|^2A+\rho \tag{S4}$$

Where $A=E\sqrt{\gamma L/\alpha}$, $t'=\alpha t/t_R$, $x=\tau\sqrt{2\alpha/\left(L\left|\beta_2\right|\right)}$, $\rho=E_0\sqrt{\gamma LT/\alpha^3}$ and $\theta=\delta_0/\alpha$. Employing the Newton-Raphson continuation algorithm, we can determine the existence

range of different dark pulse solutions. Among different dark pulse solutions, the two-soliton state with each soliton having one single dip for the real part of A, which is referred as 2×FSR 1st-order dark pulse state, is what we are interested in. The spectrum and time-domain shape are displayed in Supplementary Fig. S2c and d, whose spectra are similar to that observed in the experiment. The existence range of the 2×FSR 1st-order dark pulse state is shown in Supplementary Fig. S2a. Due to a large nonlinear coefficient and a high quality factor, the dark pulse states can be supported even with sub-milliwatt-level pump power in our devices. The existence ranges for different 2×FSR dark pulse solutions are shown in Supplementary Fig. S2b and e respectively, with pump powers of 1.58 mW and 0.93 mW. The highest steps are the existence ranges of 1st-order dark pulses. The spectra with pump powers of 1.58 mW and 0.93 mW are shown in Supplementary Fig. S2c and f, which shows great similarity to that observed in experiment.

Supplementary note III: Channel-by-channel characterizations of the large frequency chirping

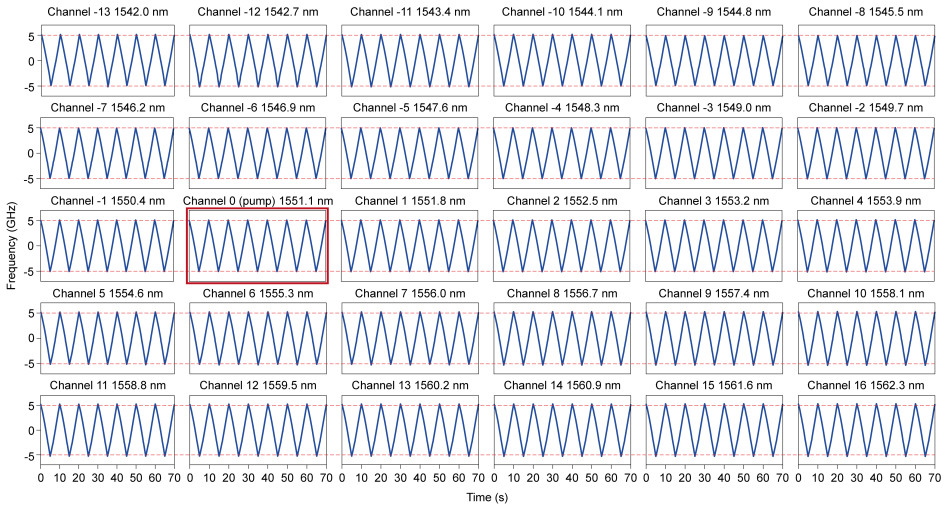

Supplementary Fig. S3: Parallel frequency chirping in mode-locked microcomb. The 10 GHz chirping transduced from the pump laser of 30 channels are measured line-by-line, ranging from 1542.0 nm to 1562.3 nm. The pump channel is outlined in red.

Channel-by-channel characterizations of the large frequency chirping in the AlGaAsOI dark-pulse microcomb is performed. The frequency spacing of the chirping microcomb is ∼

0.7 nm (single FSR). Totally 30 channels are measured, which is mainly limited by the operation bandwidth of the EDFA and WSS in the experimental link. The results show great consistency for 10 GHz symmetric triangular frequency excursion among all channels, indicating the capability for acting as a highly parallel FMCW source for Lidar. The linearity of the triangular frequency modulation signal is limited by the microwave driver, which can be further improved by compensation algorithm for piratical ranging. The frequency modulation is set to be 0.1 Hz, limited by the exposure time of the wavelength meter. The tuning speed is mainly depends on the cavity photon decay rate, and can be further achieved to $> 10^{17}$ Hz^2 by applying the chirping with a single sideband modulator (SSB) .

Supplementary note IV: Frequency noise of a DFB pumped dark-pulse micro-comb

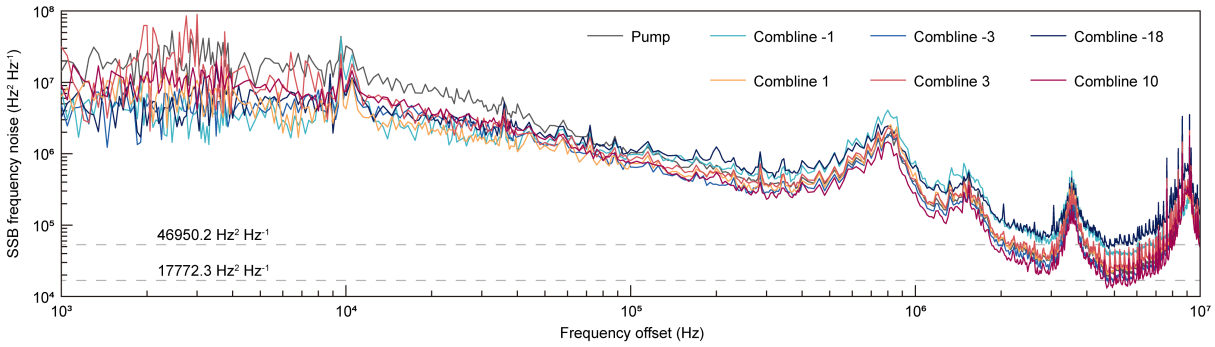

Supplementary Fig. S4: Measured single-sideband frequency noise of comb teeth in the DFB pumped scheme.

For DFB pumped dark-pulse microcomb in our AlGaAsOI resonator, the single-sideband frequency noises of the comb lines are also characterized, as shown in Supplementary Fig.4, where The same trend of comb line decoherence in ECDL pump scheme can be also found. For a DFB pump laser whose linewidth is around 100 kHz, the generated comb lines keep the coherence almost on the same order of magnitude, while the instability of the repetition rate in the free-running operation mode results in an increased intrinsic linewidth of generated comb line with the separation from the comb (i.e. the linewidth of the -18 comb line is about 2.6 times compared with that of pump). Despite this, the noise performance is enough for data communication with the speed of tens or hundreds of Gbaud and other applications

with less stringent requirements on laser linewidth.